ACS Macro Letters

Letter

pubs.acs.org/macroletters

Dimensions of Biological Cellulose Nanocrystals Maximize Fracture Strength

Robert Sinko, Shawn Mishra, Luis Ruiz, Nick Brandis, and Sinan Keten*

Department of Civil and Environmental Engineering and Department of Mechanical Engineering, Northwestern University, 2145 Sheridan Road, Room A136, Evanston, Illinois 60208, United States

Supporting Information

ABSTRACT: Cellulose nanocrystals (CNCs) exhibit outstanding mechanical properties exceeding that of Kevlar, serving as reinforcing domains in nature's toughest biological nanocomposites such as wood. To establish a molecular-level understanding of how CNCs develop high resistance to failure, here we present new analyses based on atomistic simulations on the fracture energy of Iβ CNCs. We show that the fracture energy depends on the crystal width, due to edge defects that significantly reduce the fracture energy of small crystals but have a negligible effect beyond a critical width. Additionally, collective effects of sheet stacking and stabilization by van der Waals interactions saturate at a critical crystal thickness that we predict with an analytical relationship based on a physical model. Remarkably, ideal dimensions optimizing fracture energy are found to be 4.8−5.6 nm in thickness (approximately 6−7 layers) and 6.2−7.3 nm in width (approximately 6−7 cellulose chains), which correspond to the common dimensions of CNCs found in nature. Our studies shed light on evolutionary principles that provide guidance toward high mechanical performance in natural and synthetic nanobiocomposites.

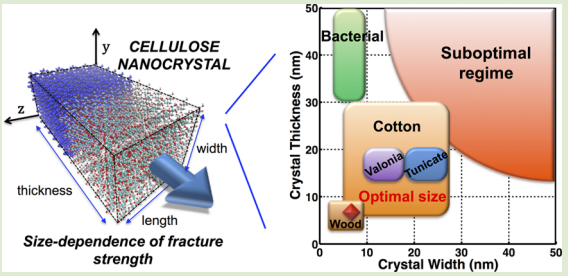

Cellulose is the most abundant organic compound and biopolymer found on our planet,[1] serving as a morphologically versatile building block for natural structural materials. The elastic modulus of cellulose nanocrystals (CNCs) exceeds 100 GPa,[2] making it a potential low-cost reinforcing filler material for nanocomposites and nanofibers. CNCs are incorporated in soft amorphous cellulose domains in wood, leading to a reinforced nanocomposite with exceptional strength and toughness (Figure 1A).[4] The low density, large aspect ratio, high axial modulus, and high specific strength[5−7] of cellulose nanocrystals and nanowhiskers arising from their nearly defect-free structure make them ideal building blocks as fillers[3,14−19] that can also be easily functionalized through compatibilizing surface modifications.[2,5,8−13] Along this line, environmentally responsive polymer−CNC nanocomposites have been manufactured to extend mechanical properties of cellulose nanocomposites to the dynamic range.[3,14,15]

Combining relatively rigid, organic nonmineralized nanocrystals with soft amorphous domains is a universal strategy for achieving strength and toughness in biomaterials like spider silk,[16,17] yet this strategy often requires the size of the reinforcing domains to be small in one or more dimensions. Whereas atomistic studies on CNCs have focused on the axial strength[7,18−20] and the interaction of CNCs with secondary molecules such as polymers or solvents,[3,21,22] the role of defects and size effects[4,10,23−27] on mechanical properties remains to be fully understood.[3] To address this issue, here we carry out an atomistic study on the nanoscale interactions in CNCs that give rise to impressive macroscale mechanical properties. We focus on a model system consisting of a single monoclinic Iβ cellulose nanocrystal, the most stable and naturally abundant CNC polymorph.[28] In recent experiments, cellulose microfibril segments were shown to peel along the [200] plane when subjected to intensive sonication,[29,30] which arguably is the weakest plane of CNCs under isotropic loading conditions. On the basis of this assumption, here we present results from tensile pulling simulations that aim to quantify the fracture strength of the [200] surface in CNCs that are commonly found in nature and in man-made cellulose nanocomposites. Using steered molecular dynamics (SMD),[31] we calculate the work required to induce fracture as the two halves of the crystal are forcibly separated (Figure 1B, and see Supporting Information for simulation setup and protocols). We then vary the dimensions of CNCs to assess the effects of size on the nanoscale fracture energy calculations. Finally, we corroborate the size-dependence effects with the typical dimensions of CNCs observed in nature.

Figure 2A illustrates the potential of mean force (PMF) or, equivalently, one-dimensional free energy landscape of CNC interactions computed from SMD simulations (see Supporting Information for details). The equilibrium distance between sheets, defined as the minimum of the energy well, is measured to be a = 3.8 Å, which is in agreement with a = 3.9 Å measured experimentally.[32] The free energy difference corresponding to the work to fracture the CNC ranges from 3500 kcal/mol (6 ×

Received: September 10, 2013
Accepted: December 9, 2013
Published: December 27, 2013

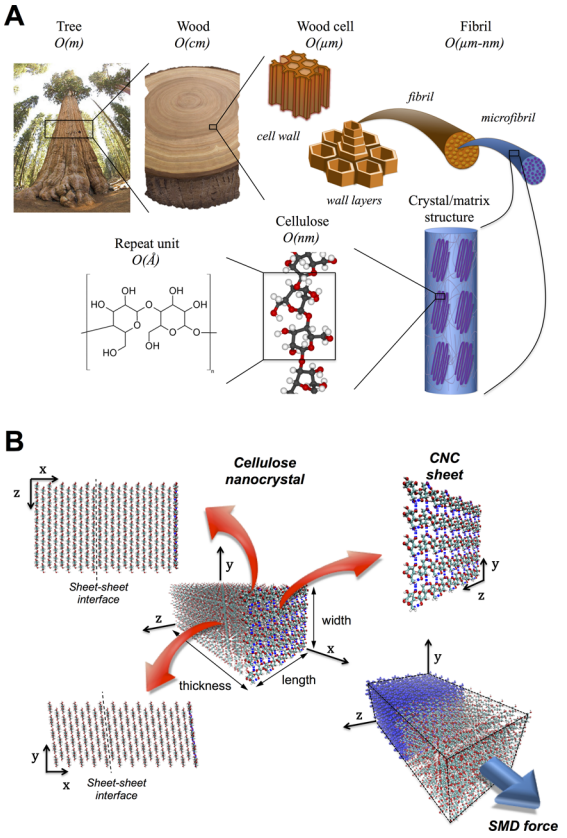

Figure 1. (A) Hierarchical structure of wood and the nanocomposite morphology involving CNCs and amorphous domains. (B) Atomistic CNC structure used in simulation, highlighting the [200] plane along which fracture occurs.

5 × 5 crystal) to 80 000 kcal/mol (6 × 15 × 20 crystal), depending on crystal size. When normalized by the cross-sectional area of the crystals, the resulting fracture energies range from approximately G = 3 to 5 kcal/mol-Å^2 (2.4−3.6 J/m^2), with surface energy values ranging from γ_s = 1.5 to 2.5 kcal/mol-Å^2 (1.2−1.8 J/m^2). The measured fracture energy is comparable to that of brittle materials such as silica glass with a fracture energy of 1−5 J/m^2 as reported experimentally.[33] The PMF can be considered as the effective intercolloidal potential between two halves of a CNC, which has never been quantified experimentally nor computationally for cellulose nanocrystals.[3] Our analysis illustrates here that while CNCs have weak interactions, their work to fracture is high at the nanoscale even though larger-scale plasticity mechanisms cannot be activated.

The potential well obtained through PMF calculations can also be utilized to compute the elastic constants and stress−strain behavior (see Supporting Information).[34] This stress−strain relationship can be considered as the nanoscale cohesive law describing the interfacial failure behavior along this plane continuously in elastic and nonlinear (large deformation) regimes. The corresponding stress−strain plot is shown in Figure 2B, which yields a transverse modulus of E_T = 20.1 GPa for the CNC in the initial linear elastic regime. The modulus value falls into the range predicted from previous simulations as well as atomic force microcopy experiments of 11−57 GPa.[35] This value is lower than the elastic modulus along the chain direction (E = 110−200 GPa[35]) because the intersheet plane is stabilized by weaker interactions compared to the covalent interactions and hydrogen bonds in the chain direction.[36−39] On the contrary, factors contributing to intersheet stability can be attributed to either (i) the large number of hydroxyl groups that facilitate intersheet hydrogen bonding[36,40] or (ii) out-of-plane van der Waals interactions between the backbone ring structures.[41,42] Analysis presented in Figure 3A clarifies the dynamics of these molecular interactions. Hydrogen bond occupancies, defined here as the percentage of time that a hydrogen bond is considered "on" during the simulation, provide a measure for the strength of cohesion along a plane, where longer bond lifetimes lead to greater fracture strength according to stochastic theories of fracture.[43,44] Whereas the hydrogen bonds stabilize the intrasheet directions and have high stability (generally greater than 90% occupancy and with double hydrogen bonding up to 200% occupancy), the intersheet hydrogen bonds are largely transient (less than 10% occupancy on average) due to the unfavorable donor−hydrogen−acceptor angle of hydroxyls orthogonal to the sheet plane. Thus, we attribute the strong interaction along the intersheet direction to hydrophobic ring−ring interactions and hydrophilic ribbons within the sheets in line with studies supporting the amphiphilic nature of cellulose sheets.[41,42,45]

The hydrogen bond occupancy is typically lower along the edges of crystals due to higher thermal fluctuations of crystals. As illustrated in Figure 3B, the average root-mean-square

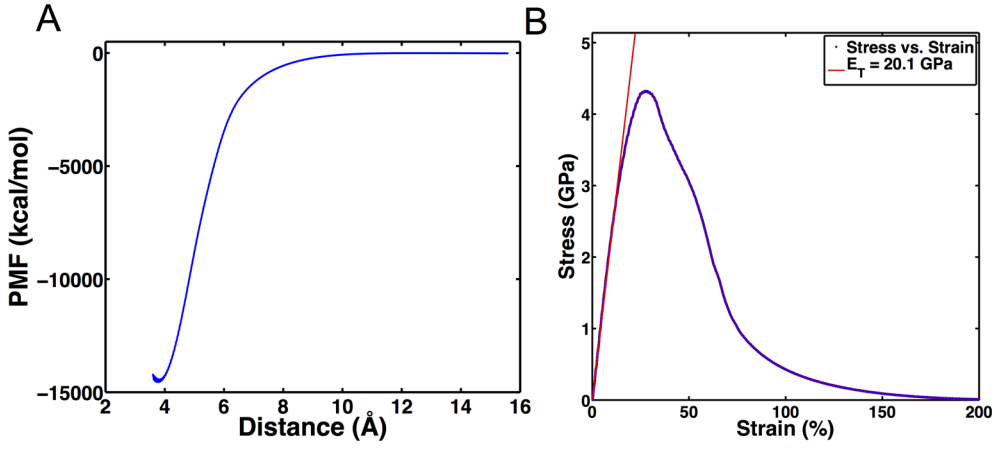

Figure 2. (A) Potential of mean force (PMF) for 2 m/s pulling of the 7 × 10 × 10 CNC, yielding a ΔE of ∼14 560 kcal/mol and (B) the stress−strain plot for the 7 × 10 × 10 crystal obtained from the PMF curve. The transverse Young's Modulus is calculated to be 20.1 GPa.

dx.doi.org/10.1021/mz400471y | ACS Macro Lett. 2014, 3, 64−69

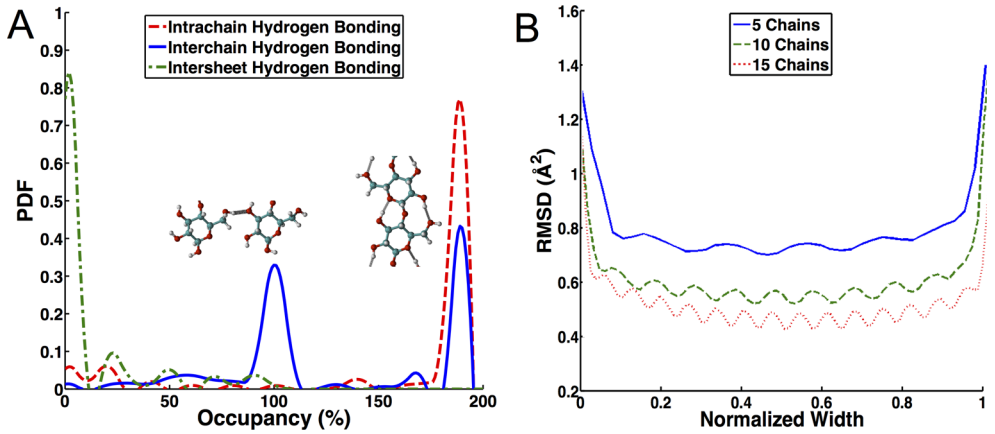

Figure 3. (A) Occupancies of interchain, intrachain, and intersheet hydrogen bonds, the first two of which are within a single cellulose sheet. Values exceed 100% when two hydrogen bonds can form. The occupancies in the intersheet direction are very low, suggesting transient hydrogen bonding. (B) Root-meat-square fluctuations for systems of increasing width. The width axis has been normalized to range from 0 to 1. Simulations indicate greater fluctuations and edge effects in small CNCs compared to larger CNCs.

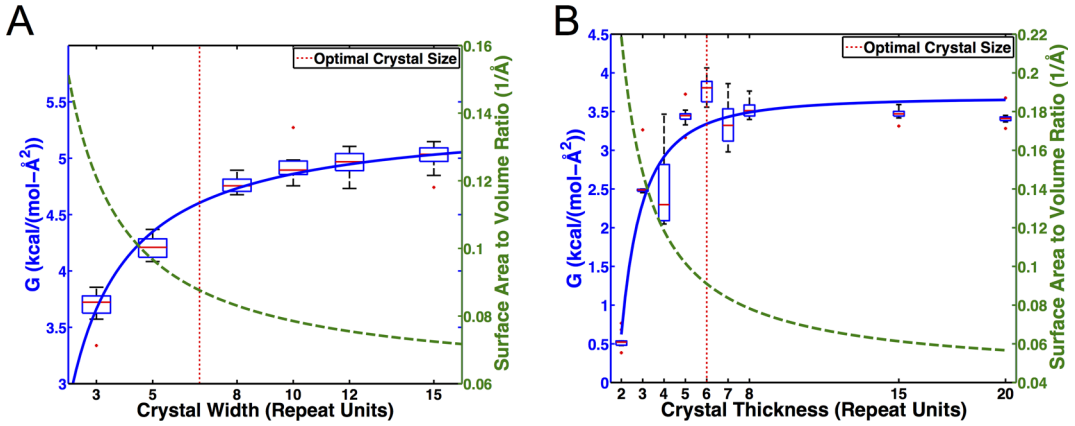

Figure 4. (A) Fracture energy, G (i.e., the force required to separate CNCs), as a function of the width of the crystals given in terms of the number of repeat units (length is 20 repeat units for all cases). The blue solid fitting line corroborates that $G \sim ((w - t)/w)$, where t denotes the size of the defect region. (B) G as a function of the thickness of the crystals in terms of the number of repeat units on each side of the fracture surface (width and length are 10 repeat units). The solid fitting follows the $G \sim 1/n^2$ scaling using H and a as material parameters. Both scaling relationships suggest that beyond the optimal crystal size (red vertical dotted line) there can be no significant increase in interfacial strength, and further, surface area to volume ratio will diminish (green dashed line).

fluctuation (RMSF) of atoms across the width for different size nanocrystals is not the same. Higher overall RMSFs observed in smaller crystals are particularly amplified near the edges, indicating greater thermal fluctuations of the atoms and thus lower stability. These unstable regions constitute a greater portion of the overall width, thereby lowering CNC stability. This implies that the ideal width of a CNC inclusion has to be large enough such that the edge defects play a lesser role and that larger CNCs have greater fracture energy. Assuming that the number of edge chains that have lower binding strength is more or less constant across all systems (having a width w), the fracture energy scaling should be size dependent and scale inversely with the width, w; that is $G \sim ((w - t)/w)$, where t denotes the size of the defect region.

To quantify whether this hypothesis is correct, we extend our SMD simulations to directly compute the fracture energy of CNCs with widths varying from 3 to 15 repeat units. Similar size-dependence studies have been carried out for silk nanocrystals and various protein structures in the past to explain the scaling of strength with molecular dimensions.[16,46] Here, the fracture energy is a key metric for cellulose materials because CNCs commonly act as physical cross-links that resist failure. Figure 4A illustrates that as the width of the CNC is increased there is an increase in the fracture energy. However, the fracture energy saturates around ~4 kcal/mol-Å^2 for a width of 10 cellulose chains, exhibiting approximately the same value for larger widths. This plateau is largely due to the edge effect described earlier and presented in Figure 3B, where bonds at the edge of the crystal serve as defects and become crack nucleation points within the crystal. In finite-sized crystals, the stacking arrangement of cellulose chains is relatively unstable (see Figure 1B for the crystal geometry) where neighboring sheets do not stabilize chains at the edges. Considering that van der Waals interactions are the dominant stabilizing force on the basis of the analysis presented in Figure 3A, we can conclude that the edges then have a lower degree of stability and serve as defect points. Simulations with 5 and 10 repeat units in length approximately have the same plateau value for the fracture energy for a crystal width of 10 chains, indicating that this width is optimized independent of the chain length (see Supporting Information).

dx.doi.org/10.1021/mz400471y | ACS Macro Lett. 2014, 3, 64–69

Next, we present an analysis for the scaling of the fracture energy with crystal thickness, which is defined as the number of sheets on each side of the fracture plane. Our study on CNCs with crystal thicknesses ranging from 2 to 20 layers (1.7 to 15.7 nm) shows a saturation effect with increasing thickness, similar to what is observed with width as shown in Figure 4B. Here we consider that the dominant force along this direction is van der Waals interactions (Figure 3A) and that the van der Waals interaction energy E_v between two parallel infinite plates separated by a distance a is given by[47]

$$E_v(a) = -\frac{H}{12\pi a^2} \tag{1}$$

where H is the Hamaker coefficient that defines the interaction strength between two surfaces in a medium. Equation 1 is a general description that requires the knowledge of surface charge distribution of the interfaces. Within CNCs, the partial charges of the repeat units, as computed from full electrostatic calculations based on the CHARMM[48,49] force field along with nonbonded interactions, govern the calculated value of H, and a = 3.8 Å is determined from the equilibrated crystal structure. To describe the scaling of the fracture energy, we need to derive an expression for the scaling of this energy with the number of sheets in a CNC. Assuming that the Hamaker coefficient is invariant at these length scales (see Supporting Information), the total interfacial energy for n stacked sheets per side along a fracture surface can be written using the following expression

$$E_v(n) = \frac{H}{12\pi a^2} \sum_{i=-n+1}^{n-1} \frac{(n - |i|)}{(i + n)^2} \tag{2}$$

Assuming a cutoff distance of eight cellulose sheets, beyond which the sheet interactions can be considered negligible, we find that this discrete summation function can be approximated by a continuous relationship of the form $E_v(n) = A - k/n^2$ (see Supporting Information). The fitting parameters also yield a prediction for Hamaker's coefficient, $H = 3.9 \times 10^{-20}$ J, which is in good agreement with experimental measurements of a cellulose thin film, $H = 5.8 \times 10^{-20}$ J.[50] Using H and a and no other fitting parameters, agreement of the model is very good with data as shown in Figure 4B. These findings provide a physical basis for why there is nearly a 4-fold increase in the fracture energy of CNCs as the thickness is increased and also explain why this increase saturates quickly beyond several nanometers. Specifically, the collective effect of the stacked cellulose sheets initially contributes greatly to fracture strength but becomes negligible beyond a critical length scale due to the decay scaling of van der Waals interactions, which we have shown to be the dominant forces along the [200] plane of CNCs.

On the basis of the analyses of width and thickness scaling of the fracture energy summarized in Figure 4, it is now possible to determine the smallest width and thickness of a CNC that maximizes the fracture energy. It should be noted here that the considerations of the crystal fracture energy alone are not sufficient to maximize fracture toughness in nanobiocomposites. The ideal nanofiller should maximize the surface to volume ratio to avoid interfacial failure, which means that nanocrystals that have the same fracture energy but smaller thickness and width will mechanically outperform larger nanocrystals.[51] Accordingly, the ideal dimension of cellulose nanocrystals must be the smallest nanocrystals that maximize the fracture energy. Since the fracture energy scales inversely with surface area to volume ratio (Figure 4), an objective approach to define an optimal dimension is needed. Here the "optimal" crystal size is then calculated in a Pareto sense[52,53] using the difference between the fracture energy and surface to volume ratio where both quantities are normalized. Considering the overlap point as the maximum value, the 80−20 Pareto rule suggests that the optimum dimensions lie at 20% of the maximum difference between the normalized fracture energy and normalized surface to volume ratio. On the basis of this concept, our theoretical calculations supported with simulation results (shown in Figure 4) suggest that the ideal dimensions of the crystal should be 6−7 chains wide and 6−7 layers thick, which corresponds to 6.2−7.3 nm wide by 4.8−5.6 nm thick CNCs. It should be noted that the optimal thickness of 6−7 layers corresponds to a total crystal thickness of 12−14 layers (as there are 6−7 layers on each side of the fracture interface). The approximate dimensions were calculated using the standard crystalline parameters of Iβ cellulose (a = 0.778 nm, b = 0.820 nm, and c = 1.0328 nm for cellulose)[3] and in the thickness dimension also take into account the added thickness of a cellulose chain (~1.5 Å). These dimensions ensure a maximum reinforcement effect of CNCs in natural and synthetic nanocomposites by achieving large surface area that transfers the load to the CNCs while resisting fracture through this large, strong interfacial plane.

Although important generally for layered nanomaterials, these findings are very interesting in the context of cellulose-based biological materials. Examining compiled experimental data on cellulose nanocrystals obtained from tunicates, wood microfibrils, bacterial CNC, and other biosources (see Table S1 in the Supporting Information and Figure 5),[3,28] it is clear that

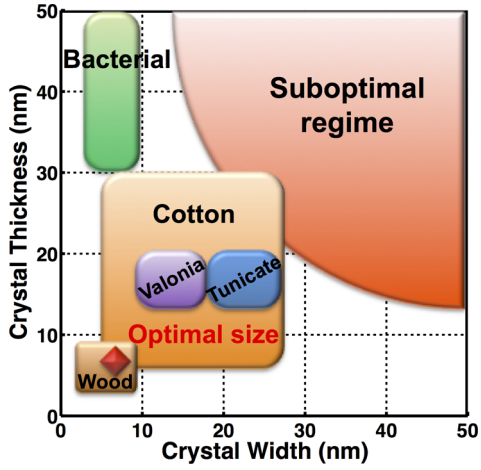

Figure 5. Schematic showing typical crystal sizes as they appear in nature compared to the optimal size discerned through MD (red diamond).

CNCs embedded in amorphous domains in biological structural materials often have width and height around a few nanometers, rarely exceeding 10 nm. This concept is intriguing, and given that the natural use of cellulose involves structural support, it is conceivable that the conserved size of these systems follows a mechanical design principle that is aimed at finding CNCs that achieve the highest fracture energy while maximizing surface area to volume ratio. The optimal dimensions obtained with this simple consideration are

dx.doi.org/10.1021/mz400471y | ACS Macro Lett. 2014, 3, 64−69

illustrated in Figure 5, showing very good agreement with observations of natural CNCs. In some biological systems such as wood, the so-called elementary size of cellulose is an arrangement of 36 individual cellulose chains[28] to form what are termed elementary fibrils and have dimensions ranging from approximately 2.5 to 3.5 nm.[54] Our findings here suggest that the optimal size from a fracture perspective is close to this value but slightly greater, perhaps involving larger assemblies of the basic building blocks.

Our studies build on earlier works that suggested nanoconfinement and flaw tolerance as important natural design principles for creating strong and tough materials,[1,55−58] although illustrating different mechanisms in the case of CNCs. The optimal dimensions of CNCs arise directly from the sheet geometry and the scaling nature of the universal van der Waals molecular interactions along the [200] plane—two key bottom-up design parameters in nature. The methodology for computing fracture energies and the size dependence in nanostructures pave the way for understanding collective fracture energy scaling in other systems, such as peptide assemblies and functionalized graphene sheets. Extending this work to functionalized CNC assemblies and polymer interfaces will reveal key insight into blending disparate material building blocks into next-generation functional materials built by nature and assembled following nature's own evolutionary design principles.

■ ASSOCIATED CONTENT

Supporting Information

Simulation protocols and fracture energy calculations are provided. This material is available free of charge via the Internet at http://pubs.acs.org.

■ AUTHOR INFORMATION

Corresponding Author

*E-mail: s-keten@northwestern.edu.

Author Contributions

The manuscript was written through contributions of all authors. R.S. and S.M. contributed equally to this work. All authors have given approval to the final version of the manuscript.

Notes

The authors declare no competing financial interest.

■ ACKNOWLEDGMENTS

The authors acknowledge funding from the National Science Foundation (award # CBET-1234305) and the Army Research Office (award # W911NF-13-1-0241). Authors acknowledge support from the Departments of Civil and Environmental Engineering and Mechanical Engineering at Northwestern University, as well as a supercomputing grant from Northwestern University High Performance Computing Center. R. S. was supported by the Department of Defense (DoD) through the National Defense Science & Engineering Graduate Fellowship (NDSEG) Program. We thank Dominique Derome (EMPA), Jan Andzelm (ARL), Robert Moon and Pablo Zavattieri (Purdue University) for insightful discussions on cellulose nanocomposites.

■ REFERENCES

(1) Fratzl, P.; Weinkamer, R. *Prog. Mater. Sci.* **2007**, *52* (8), 1263−1334.

(2) Šturcová, A.; Davies, G. R.; Eichhorn, S. J. *Biomacromolecules* **2005**, *6* (2), 1055−1061.

(3) Moon, R. J.; Martini, A.; Nairn, J.; Simonsen, J.; Youngblood, J. *Chem. Soc. Rev.* **2011**, *40* (7), 3941−3994.

(4) Postek, M. T.; Vladár, A.; Dagata, J.; Farkas, N.; Ming, B.; Wagner, R.; Raman, A.; Moon, R. J.; Sabo, R.; Wegner, T. H. *Meas. Sci. Technol.* **2011**, *22* (2), 024005.

(5) Eichhorn, S.; Davies, G. *Cellulose* **2006**, *13* (3), 291−307.

(6) Imam, S. H.; Greene, R. V.; Zaidi, B. R. *Biopolymers: utilizing nature's advanced materials*; American Chemical Society: Washington, DC, 1999.

(7) Tashiro, K.; Kobayashi, M. *Polymer* **1991**, *32* (8), 1516−1526.

(8) Beck-Candanedo, S.; Roman, M.; Gray, D. G. *Biomacromolecules* **2005**, *6* (2), 1048−1054.

(9) Dong, X. M.; Revol, J. F.; Gray, D. G. *Cellulose* **1998**, *5* (1), 19−32.

(10) Hubbe, M. A.; Rojas, O. J.; Lucia, L. A.; Sain, M. *Bioresources* **2008**, *3* (3), 929−980.

(11) Padalkar, S.; Capadona, J. R.; Rowan, S. J.; Weder, C.; Won, Y.-H.; Stanciu, L. A.; Moon, R. J. *Langmuir* **2010**, *26* (11), 8497−8502.

(12) Rusli, R.; Eichhorn, S. J. *Appl. Phys. Lett.* **2008**, *93*, 3.

(13) Spoljaric, S.; Genovese, A.; Shanks, R. A. *Compos., Part A: Appl. Sci. Manuf.* **2009**, *40* (6−7), 791−799.

(14) Shanmuganathan, K.; Capadona, J. R.; Rowan, S. J.; Weder, C. *J. Mater. Chem.* **2010**, *20* (1), 180−186.

(15) Derome, D.; Griffa, M.; Koebel, M.; Carmeliet, J. *J. Struct. Biol.* **2011**, *173* (1), 180−190.

(16) Keten, S.; Xu, Z. P.; Ihle, B.; Buehler, M. J. *Nat. Mater.* **2010**, *9* (4), 359−367.

(17) Keten, S.; Buehler, M. J. *Nano Lett.* **2008**, *8* (2), 743−748.

(18) Dri, F.; Hector, L. G., Jr.; Moon, R. J.; Zavattieri, P.D. *Cellulose* **2013**, *20* (6), 2703−2718.

(19) Neyertz, S.; Pizzi, A.; Merlin, A.; Maigret, B.; Brown, D.; Deglise, X. *J. Appl. Polym. Sci.* **2000**, *78* (11), 1939−1946.

(20) Tanaka, F.; Iwata, T. *Cellulose* **2006**, *13* (5), 509−517.

(21) Mazeau, K.; Vergelati, C. *Langmuir* **2002**, *18* (5), 1919−1927.

(22) Yui, T.; Nishimura, S.; Akiba, S.; Hayashi, S. *Carbohydr. Res.* **2006**, *341* (15), 2521−2530.

(23) Capadona, J. R.; Shanmuganathan, K.; Trittschuh, S.; Seidel, S.; Rowan, S. J.; Weder, C. *Biomacromolecules* **2009**, *10* (4), 712−716.

(24) Morán, J. I.; Alvarez, V. A.; Cyras, V. P.; Vázquez, A. *Cellulose* **2008**, *15* (1), 149−159.

(25) Chen, Y.; Liu, C.; Chang, P. R.; Cao, X.; Anderson, D. P. *Carbohydr. Polym.* **2009**, *76* (4), 607−615.

(26) Saito, T.; Kuramae, R.; Wohlert, J.; Berglund, L. A.; Isogai, A. *Biomacromolecules* **2012**, *14* (1), 248−253.

(27) Eichhorn, S. J. *ACS Macro Lett.* **2012**, *1* (11), 1237−1239.

(28) Habibi, Y.; Lucia, L. A.; Rojas, O. J. *Chem. Rev.* **2010**, *110* (6), 3479−3500.

(29) Li, Q.; Renneckar, S. *Cellulose* **2009**, *16* (6), 1025−1032.

(30) Li, Q.; Renneckar, S. *Biomacromolecules* **2011**, *12* (3), 650−659.

(31) Park, S.; Khalili-Araghi, F.; Tajkhorshid, E.; Schulten, K. *J. Chem. Phys.* **2003**, *119*, 3559.

(32) ImCi, T.; Putaux, J.-L.; Sugiyama, J. *Polymer* **2003**, *44* (6), 1871−1879.

(33) Wiederho, Sm. *J. Am. Ceram. Soc.* **1969**, *52* (2), 99−&.

(34) Ruiz, L.; Keten, S. *J. Eng. Mech.* **2012**, DOI: http://dx.doi.org/10.1061/(ASCE)EM.1943-7889.0000471.

(35) Lahiji, R. R.; Xu, X.; Reifenberger, R.; Raman, A.; Rudie, A.; Moon, R. J. *Langmuir* **2010**, *26* (6), 4480−4488.

(36) Azizi Samir, M. A. S.; Alloin, F.; Dufresne, A. *Biomacromolecules* **2005**, *6* (2), 612−626.

(37) Dufresne, A. *J. Nanosci. Nanotechnol.* **2006**, *6* (2), 322−330.

(38) Kong, K.; Eichhorn, S. J. *J. Macromol. Sci., Part B* **2005**, *44* (6), 1123−1136.

(39) Nishiyama, Y.; Langan, P.; Chanzy, H. *J. Am. Chem. Soc.* **2002**, *124* (31), 9074−9082.

(40) Bodvik, R.; Dedinaite, A.; Karlson, L.; Bergström, M.; Bäverbäck, P.; Pedersen, J. S.; Edwards, K.; Karlsson, G.; Varga, I.; Claesson, P. M. *Colloids Surf., A* **2010**, *354* (1), 162−171.
(41) Biermann, O.; Hädicke, E.; Koltzenburg, S.; Müller-Plathe, F. *Angew. Chem., Int. Ed.* **2001**, *40* (20), 3822−3825.
(42) Lindman, B.; Karlström, G.; Stigsson, L. *J. Mol. Liq.* **2010**, *156* (1), 76−81.
(43) Ruiz, L.; VonAchen, P.; Lazzara, T. D.; Xu, T.; Keten, S. *Nanotechnology* **2013**, *24*, 19.
(44) Bell, G. *Science* **1978**, *200* (4342), 618−627.
(45) Yamane, C.; Aoyagi, T.; Ago, M.; Sato, K.; Okajima, K.; Takahashi, T. *Polym. J* **2006**, *38* (8), 819−826.
(46) Nova, A.; Keten, S.; Pugno, N. M.; Redaelli, A.; Buehler, M. J. *Nano Lett* **2010**, *10* (7), 2626−2634.
(47) Israelachvili, J. N. *Intermolecular and surface forces*, revised third ed.; Academic Press: New York, 2011.
(48) Brooks, B. R.; Bruccoleri, R. E.; Olafson, B. D.; States, D. J.; Swaminathan, S.; Karplus, M. *J. Comput. Chem.* **1983**, *4* (2), 187−217.
(49) Raman, E. P.; Guvench, O.; MacKerell, A. D. *J. Phys. Chem.* **2010**, *114* (40), 12981−12994.
(50) Bergstrom, L.; Stemme, S.; Dahlfors, T.; Arwin, H.; Odberg, L. *Cellulose* **1999**, *6* (1), 1−+.
(51) Ajayan, P. M.; Schadler, L. S.; Braun, P. V. *Nanocomposite science and technology*; Wiley: New York, 2006.
(52) Chen, Y. S.; Chong, P. P.; Tong, Y. G. *Scientometrics* **1993**, *28* (2), 183−204.
(53) Ackbarow, T.; Chen, X.; Keten, S.; Buehler, M. J. *Proc. Natl. Acad. Sci.* **2007**, *104* (42), 16410−16415.
(54) Zhang, Y. Z.; Chen, X. L.; Liu, J.; Gao, P. J.; Shi, D. X.; Pang, S. J. *J. Vac. Sci. Technol. B* **1997**, *15* (4), 1502−1505.
(55) Buehler, M. J.; Yao, H. M.; Ji, B. H.; Gao, H. J. Atomistic and continuum studies of flaw tolerant nanostructures in biological systems. In *Mechanical Properties of Bioinspired and Biological Materials*; Viney, C., Katti, K., Ulm, F. J., Hellmich, C., Eds.; Cambridge University Press: New York, 2005; Vol. *844*, pp 207−212.
(56) Fratzl, P. *J. R. Soc. Interface* **2007**, *4* (15), 637−642.
(57) Gao, H.; Ji, B.; Buehler, M. J.; Yao, H. *Mech. Chem. Biosyst.: MCB* **2004**, *1* (1), 37−52.
(58) Gao, H. J.; Ji, B. H.; Jager, I. L.; Arzt, E.; Fratzl, P. *Proc. Natl. Acad. Sci. U.S.A.* **2003**, *100* (10), 5597−5600.